Theor. Comput. Fluid Dyn. (2014) 28:1–21
DOI 10.1007/s00162-012-0286-6

ORIGINAL ARTICLE

Zhen Li Chen · Stefan Hickel · Antoine Devesa · Julien Berland · Nikolaus A. Adams

Wall modeling for implicit large-eddy simulation and immersed-interface methods

Received: 11 October 2010 / Accepted: 13 September 2012 / Published online: 21 March 2013

Abstract We propose and analyze a wall model based on the turbulent boundary layer equations (TBLE) for implicit large-eddy simulation (LES) of high Reynolds number wall-bounded flows in conjunction with a conservative immersed-interface method for mapping complex boundaries onto Cartesian meshes. Both implicit subgrid-scale model and immersed-interface treatment of boundaries offer high computational efficiency for complex flow configurations. The wall model operates directly on the Cartesian computational mesh without the need for a dual boundary-conforming mesh. The combination of wall model and implicit LES is investigated in detail for turbulent channel flow at friction Reynolds numbers from $Re_\tau = 395$ up to $Re_\tau = 100{,}000$ on very coarse meshes. The TBLE wall model with implicit LES gives results of better quality than current explicit LES based on eddy viscosity subgrid-scale models with similar wall models. A straightforward formulation of the wall model performs well at moderately large Reynolds numbers. A logarithmic-layer mismatch, observed only at very large Reynolds numbers, is removed by introducing a new structure-based damping function. The performance of the overall approach is assessed for two generic configurations with flow separation: the backward-facing step at $Re_h = 5{,}000$ and the periodic hill at $Re_H = 10{,}595$ and $Re_H = 37{,}000$ on very coarse meshes. The results confirm the observations made for the channel flow with respect to the good prediction quality and indicate that the combination of implicit LES, immersed-interface method, and TBLE-based wall modeling is a viable approach for simulating complex aerodynamic flows at high Reynolds numbers. They also reflect the limitations of TBLE-based wall models.

Keywords Large-eddy simulation · Wall model · Turbulent boundary layer equations · Immersed-boundary method

Communicated by S. Sarkar.

Z. L. Chen · S. Hickel (✉) · A. Devesa · J. Berland · N. A. Adams
Institute of Aerodynamics and Fluid Mechanics, Technische Universität München,
85748 Garching, Germany
E-mail: sh@tum.de
Tel.: +49-89-289-16140
Fax: +49-89-289-16139

Z. L. Chen
E-mail: zhenli.chen@aer.mw.tum.de

Present address
Z. L. Chen
Institute of Fluid Dynamics, Northwestern Polytechnical University,
Xi'an 710072, Shaanxi, People's Republic of China

1 Introduction

Subgrid-scale (SGS) model development for large-eddy simulation (LES) mainly follows the explicit modeling paradigm, where functional or structural concepts are invoked for devising approximations of the SGS stress tensor or for approximating the small-scale field. Less within the focus of physically motivated SGS modeling is the implicit modeling paradigm [23]. Implicit SGS models have been considered as inferior to explicit models by construction since SGS dissipation was generated essentially without strict physical motivation by nonlinear numerical stabilization mechanisms, for example, such as that provided by shock-capturing schemes. It has been shown by Garnier et al. [21] that a straightforward application of shock-capturing schemes for implicit LES in general does not lead to good results. Despite theoretical limitations, in practice, however, often good results with such implicit SGS models have been obtained [20]. As described by Grinstein et al. [23], methods for analyzing the effective SGS model provided by the underlying discretization scheme have become available. A systematic approach for a general, nonlinear discretization framework that allows for physically consistent implicit SGS modeling has been introduced by Hickel et al. [27], based on the approximate deconvolution concept [46]. The adaptive local deconvolution method (ALDM) is nonlinear and solution adaptive and incorporates a physically consistent implicit SGS model, that is, a model that recovers the subgrid-scale energy transfer in agreement with theoretical predictions for isotropic turbulence. The validity of the developed implicit model has been demonstrated for a wide range of increasingly complex flows, see e.g., [26,24].

Despite the fact that ALDM gives improved predictions of turbulence anisotropy compared with common explicit SGS models [24], the fundamental problem of having to resolve the near-wall region in turbulent flows is shared with all other implicit or explicit LES approaches. A wall-resolving LES needs to represent the near-wall anisotropy of turbulence which requires a sufficient grid resolution, scaling with the friction Reynolds number Re_τ^2 [4]. A high near-wall resolution implies a severe time step constraint, not only for numerical stability of conditionally stable time integration schemes but also for a proper resolution of turbulent transfer mechanisms. For relaxing these constraints, the concept of wall modeling has been introduced early in the development of LES methods [16,45]. With wall-modeling approaches, approximate boundary conditions and wall layer models are employed that imply resolution requirements following exterior flow scaling as $Re^{0.4}$ [41]. An essential assumption for wall modeling is a timescale separation between the near-wall turbulence dynamics and that of the exterior flow. Based on this assumption, the near-wall layer couples only weakly to the exterior flow and its evolution can be computed on the larger exterior flow timescale [29]. An obvious question is what is the simplest possible coupling model between exterior and near-wall flow. For the synthetic boundary conditions shifted to a plane away from the wall, proposed by Baggett [3], Dirichlet velocity boundary conditions are sufficient for an accurate exterior flow; however, the imposed velocity needs to have correct spectral distributions of auto- and cross-correlations. For passing information about near-wall turbulence structure to the exterior flow, one usually estimates the wall stress, as it leads to simple and robust synthetic boundary data. Commonly, the wall-parallel stress components are imposed, while the wall-normal velocity component is set to zero. Alternative approaches employing approximation theory, such as the filtered representation of the boundary condition [8], have led to considerable new insight but have not yet resulted in practically useful wall models.

A generic form of the wall stress model can be written as

$$\boldsymbol{\tau}_w = f(\mathbf{u}_o, p_o, \nu, \mathbf{x}), \tag{1}$$

where f is used to relate the wall stress $\boldsymbol{\tau}_w$ in wall-parallel directions to the velocity $\mathbf{u}_o$ and pressure p_o of the exterior flow at the coupling position $\mathbf{x} = (x_1, x_2, x_3)$. For f, algebraic closures have been proposed [16,42,45]. An alternative is to derive a closure from the turbulent boundary layer equations (TBLE) with a simple algebraic turbulence model [6,50]. More sophisticated is a hybrid approach between LES and the full Reynolds-averaged Navier–Stokes equations (RANS), see [19]. Hybrid RANS/LES methods are beyond the scope of this paper and thus are not further discussed here. Cabot [12] stated that using the precise wall stresses from resolved LES instead of those given by a wall model had little effect on the exterior flow evolution along a backward-facing step. One can conclude that SGS modeling errors and numerical errors for the exterior flow contribute to unsatisfactory predictions [40]. A wall model based on suboptimal control theory has been proposed to compensate for such errors [39]. Although improved results have been obtained, the need for a priori knowledge for defining the cost function and the increased computational load have prevented a widespread use of this approach.

So far, wall models are almost exclusively used in combination with explicit SGS models and on body-conforming structured meshes. A notable exception to the former observation is the work of Grinstein and Fureby, see [22]. A detailed investigation of wall models within the framework of implicit LES has not yet been performed to the authors' knowledge.

A practical issue is that of performing LES for flows in or around complex geometries. LES on unstructured meshes is ill advised, as the numerical truncation error can exhibit large local variations and pollutes the effect of either implicit or explicit SGS models. Structured, curvilinear meshes are hard to generate for complex geometries. An alternative is provided by immersed-interface methods where the boundary is mapped onto a, usually Cartesian, mesh [37]. In particular, for implicit LES approaches, where the spatial truncation error of the discretization scheme functions as SGS model, regular meshes are desirable, so that a benefit from using immersed-interface methods for the representation of complex boundaries can be expected, see also [36].

There are only very few published papers focusing on the wall modeling for LES in the framework of immersed-boundary (IB) methods, although the IB technique itself is rather well established [37]. A wall model based on simplified TBLE that keeps only the diffusive term, the so-called equilibrium stress balance model, has been proposed by Tessicini et al. [48] and applied to a hydrofoil flow at high Reynolds numbers, for which improved mean velocities compared to coarse LES without wall model are observed. Several additional applications of this model were presented by Cristallo and Verzicco in Ref. [15], where also the detailed finite difference implementation of the filtered Navier–Stokes equations is discussed. Choi et al. [14] have used a power law function to interpolate the velocities in the wall-normal direction, which is claimed to be suitable for high Reynolds number flow simulations. Roman et al. [44] carried out a detailed investigation for plane turbulent channel flow using the immersed-boundary method on both Cartesian and curvilinear grids. It was found that in this method, the location and the particular choice of the velocity reconstruction at the coupling position can crucially affect the predicted mean-velocity profiles. We want to emphasize that, to the best of our knowledge, all previously published methods are based on discrete-forcing or penalty techniques using local velocity reconstructions in the framework of finite difference implementations [15,17]. Such procedures generally do not satisfy mass conservation near the immersed boundary, as the filtered Navier–Stokes equations are not solved in the entire flow domain but only down to the first or second off-wall points. Exact mass conservation, however, can be essential for accurate turbulent-flow predictions [32].

In this work, the Navier–Stokes equations are solved by a finite volume method. Wall boundaries that do not conform with grid lines are consistently modeled by a conservative immersed-interface method (CIIM) [35], which is fully conservative by construction. CIIM follows the cut cell approach, that is, the finite volume flux balance of cells that are cut by the wall interface is discretized in such a way that only the fluid part of the cell contributes to the solution. When a wall model is employed, the effect of the wall shear force is imposed on the exterior LES through the interface interaction term within the underlying conservative framework of the finite volume method.

Explicit SGS models, such as the constant-coefficient Smagorinsky model used by Roman et al. [44] or the dynamic Smagorinsky model used in Refs. [15,48], are strongly affected by discretization errors in the comparably large near-wall cells typically used in wall-modeled LES, and therefore cannot account properly for the anisotropic SGS turbulence in this region. In the present work, the implicit SGS model ALDM [27] is used, which by construction is based on exploiting truncation errors for physically consistent SGS modeling. In Ref. [24], it has been shown that ALDM yields grid convergent and accurate results for wall-bounded turbulence at moderate Reynolds numbers even on very coarse grids. It is therefore expected that the combination of ALDM and CIIM offers high efficiency and more reliability for complex flow configurations.The importance of near-wall SGS modeling especially at high Reynolds number will be discussed in the following sections.

One objective of this paperis to investigate the detailed behavior of a wall model based on the simplified TBLE within ALDM-based implicit LES. For this particular purpose, turbulent channel flow is considered at friction Reynolds numbers up to $Re_\tau = 1.0 \times 10^5$. The other purpose is to formulate a TBLE-based wall model for immersed-interface methods without employing a dual-mesh approach, similarly as in Ref. [48]. As another difference to previous methods, the approach pursued in this paper employs a conservative immersed-boundary method and a TBLE-based wall model that includes the pressure gradient and time acceleration term. The overall performanceof the method is assessed for complex generic flows, the backward-facing step [31], and the periodic hill [18].

2 Implicit LES and conservative immersed-interface method

ALDM is a finite volume approach based on a nonlinear deconvolution operator and a numerical flux function, where the spatial truncation error functions as physically consistent implicit SGS model [27]. Efficient simulations of turbulent flows along complex geometries are achieved by the conservative immersed-interface method [35]. In the following, these methods are briefly described for completeness.

The Navier–Stokes equations for an incompressible fluid with uniform density are written in non-dimensional form as

$$\frac{\partial \mathbf{u}}{\partial t} + \nabla \cdot \mathbf{F}(\mathbf{u}) + \nabla p - \nu \nabla^2 \mathbf{u} = \mathbf{0}, \tag{2}$$

with $\mathbf{F}(\mathbf{u}) = \mathbf{uu}$ and $\nu = 1/Re$. The incompressible continuity equation is

$$\nabla \cdot \mathbf{u} = 0. \tag{3}$$

The differential equations for the resolved scales are obtained by applying the filter $\mathbf{G}(\mathbf{x})$ to the Eqs. (2) and (3)

$$\frac{\partial \overline{\mathbf{u}}}{\partial t} + \mathbf{G} * \nabla \cdot \mathbf{F}(\mathbf{u}) + \nabla \overline{p} - \nu \nabla^2 \overline{\mathbf{u}} = \mathbf{0}, \tag{4a}$$

$$\nabla \cdot \overline{\mathbf{u}} = 0, \tag{4b}$$

where the filtered velocity and pressure are obtained by convolution with the filter kernel: $\overline{\mathbf{u}} = \mathbf{u} * \mathbf{G}$. Applying ALDM to the Eqs. (4), where finite volume averaging functions as real-space top-hat filter, one obtains

$$\frac{\partial \overline{\mathbf{u}}_\mathbf{N}}{\partial t} + \widetilde{\mathbf{G}} * \widetilde{\nabla} \cdot \widetilde{\mathbf{F}}_\mathbf{N}(\widetilde{\mathbf{u}}_\mathbf{N}) + \nabla \overline{p}_N - \nu \nabla^2 \overline{\mathbf{u}}_\mathbf{N} = \mathbf{0}, \tag{5a}$$

$$\nabla \cdot \overline{\mathbf{u}}_\mathbf{N} = 0. \tag{5b}$$

The subscript $\mathbf{N}$ indicates the discrete approximation. $\widetilde{\mathbf{u}}_\mathbf{N}$ is the approximate deconvolution of $\overline{\mathbf{u}}_\mathbf{N}$. $\widetilde{\nabla}$ represents the discrete approximation of the divergence operator. $\widetilde{\mathbf{F}}_\mathbf{N}$ is a consistent numerical flux function

$$\widetilde{\mathbf{F}}_\mathbf{N} = \mathbf{F}((\widetilde{\mathbf{u}}_\mathbf{N}^+ + \widetilde{\mathbf{u}}_\mathbf{N}^-)/\mathbf{2}) - \boldsymbol{\sigma} |\delta \overline{\mathbf{u}}_\mathbf{N}| (\delta \widetilde{\mathbf{u}}_\mathbf{N}), \tag{6}$$

in which

$$\begin{aligned} \boldsymbol{\sigma}_{i,j,k} &= \sigma \left(\frac{L_0}{\Delta_0} \frac{\Delta \mathbf{x}_{i,j,k}}{L_{i,j,k}} \right)^{-1/3}, \\ \delta \overline{\mathbf{u}}_{i+\frac{1}{2},j,k} &= \overline{\mathbf{u}}_{i+1,j,k} - \overline{\mathbf{u}}_{i,j,k}, \\ \delta \widetilde{\mathbf{u}}_{i+\frac{1}{2},j,k} &= \widetilde{\mathbf{u}}_{i+1,j,k}^- - \widetilde{\mathbf{u}}_{i,j,k}^+. \end{aligned} \tag{7}$$

$\Delta \mathbf{x}_{i,j,k}$ are the grid spacings in the three coordinate directions. A compensation of variable grid spacing for the isotropic model parameter $\sigma = 0.069$ is achieved by L_0 and Δ_0, denoting a reference integral length scale and a reference grid size, respectively. For wall-bounded flows, the length scale $L_{i,j,k}$ is damped by

$$L_{i,j,k} = L_0 \left(1 - \exp \left[- \left(\frac{l_w u_\tau}{50\nu} \right)^3 \right] \right), \tag{8}$$

where l_w is the wall distance and u_τ is the friction velocity calculated from a general wall function [24]. In the following, we refer to Eq. (7) with Eq. (8) as van Driest (VD) damping.

Equations (5) are solved on a staggered Cartesian mesh, and a pressure projection method is used. An explicit third-order Runge-Kutta scheme is used for time advancement. The time step is dynamically adapted to satisfy a Courant-Friedrichs-Lewy (CFL) condition with CFL = 1.0. The pressure Poisson equation and diffusive terms are discretized by second-order central differences, whereas the convective terms are discretized by a simplified formulation of ALDM for improved computational efficiency [25].

In the framework of immersed-interface method, for the normal cells away from the immersed interface, the Eqs. (5) reduce to normal finite volume method. However, for the cells cut by the immersed interface, the

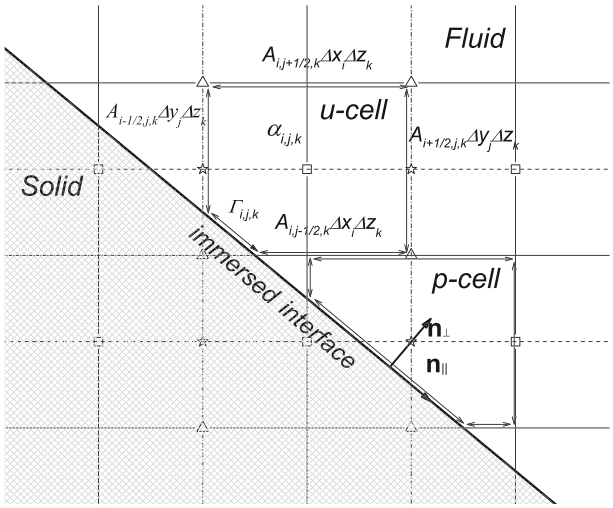

Fig. 1 Flux calculation on a cut cell

fluxes through the interface have to be included and the fluxes at cell faces must be corrected. The Eqs. (5a) for one cut cell are modified as

$$\frac{\partial \overline{\mathbf{u}}_{i,j,k}}{\partial t} + \frac{1}{V_{i,j,k}} \sum_{\partial \mathbf{I}_{i,j,k}} [\widetilde{\mathbf{F}}(\widetilde{\mathbf{u}}_{\mathbf{N}}) - \nu \nabla(\overline{\mathbf{u}})] \cdot \mathbf{n} \Delta S + \nabla \overline{p}_{i,j,k} + \mathbf{M}_{i,j,k} = \mathbf{0}. \tag{9}$$

The control volume $V_{i,j,k}$ immersed in the fluid is computed using the volume fraction $\alpha_{i,j,k}$,

$$V_{i,j,k} = \alpha_{i,j,k} \Delta x_i \Delta y_j \Delta z_k. \tag{10}$$

The area of cell faces ΔS immersed within the fluid is obtained by the face apertures $A_{l,m,n}$, as sketched in Fig. 1,

$$\Delta S = \begin{cases} A_{i-\frac{1}{2},j,k} \Delta y_j \Delta z_k, & \text{west,} \\ A_{i+\frac{1}{2},j,k} \Delta y_j \Delta z_k, & \text{east,} \\ A_{i,j-\frac{1}{2},k} \Delta x_i \Delta z_k, & \text{south,} \\ A_{i,j+\frac{1}{2},k} \Delta x_i \Delta z_k, & \text{north,} \\ A_{i,j,k-\frac{1}{2}} \Delta x_i \Delta y_j, & \text{back,} \\ A_{i,j,k+\frac{1}{2}} \Delta x_i \Delta y_j, & \text{front,} \\ \Gamma_{i,j,k}, & \text{immersed interface.} \end{cases} \tag{11}$$

The convective fluxes and diffusive fluxes are calculated at the face centers of cut cells as with normal fluid cells, which allows the computation to use ALDM and central discretization scheme without modification. The convective flux $\mathbf{C}_{\Gamma_{i,j,k}}$ across the immersed interface

$$\mathbf{C}_{\Gamma_{i,j,k}} = \widetilde{\mathbf{F}}(\widetilde{\mathbf{u}}_{\mathbf{N}})|_{\Gamma_{i,j,k}} \cdot \mathbf{n} \Gamma_{i,j,k} \tag{12}$$

can be directly calculated when the Dirichlet boundary conditions are used. It is exactly zero when applying a no-slip boundary condition. The diffusive flux $\mathbf{D}_{\Gamma_{i,j,k}}$ across the immersed interface can be calculated from the wall shear stress as

$$\mathbf{D}_{\Gamma_{i,j,k}} = -\nu \nabla(\overline{\mathbf{u}})|_{\Gamma_{i,j,k}} \cdot \mathbf{n} \Gamma_{i,j,k} = \boldsymbol{\tau}_w \Gamma_{i,j,k}. \tag{13}$$

Small cut cells, typically cells with $\alpha_{i,j,k} < 0.5$, undergo a special treatment by mixing their momentum with their neighbor cells in a conservative fashion, in order to prevent more severe numerical stability restrictions. For very small cut cells that do not contribute to the pressure Poisson equation, the impermeability

condition of the interface cannot be achieved by a Neumann condition for the pressure, but by an acceleration of the wall-normal velocity to satisfy the wall-normal momentum balance. This is accomplished by a momentum-exchange term in the wall-normal direction

$$\mathbf{M}_{i,j,k} = -\frac{\overline{\mathbf{u}}_{\perp,i,j,k}}{\Delta t}. \tag{14}$$

For the details of the momentum-mixing procedure and the pressure Poisson equation modification, see Ref. [35]. The remaining issue is modeling of the wall shear stress $\boldsymbol{\tau}_w$, which is detailed in the next section.

3 Wall model for immersed-interface methods

For determining the wall stress in Eqs. (1, 13), several modeling approaches are possible. It appears that a good compromise between accuracy and computational cost is to determine the wall stress from the TBLE, solved in a near-wall region. This procedure belongs to the two-layer modeling approaches, introduced by Balaras et al. [5]. Basic assumption for the validity of the TBLE in the near-wall region is a temporal scale separation between the exterior flow and the near-wall flow, where also the boundary layer assumptions hold (slow changes in wall-parallel directions, fast changes in wall-normal direction). The TBLE are further simplified by dropping convective terms, as friction and pressure effects are expected to be dominant. This assumption is critical for the choice of the coupling position between LES and TBLE. If it is far from the edge of the buffer layer, the simplified TBLE fail to include strong convection effects of the outer layer. If it is too close to the wall, the buffer layer is adversely affected. For our method, we have established that the proper coupling position is in the lower range of the logarithmic layer for developed channel flow. The following simplified unsteady TBLE are used

$$\frac{\partial}{\partial x_2}(\nu + \nu_t)\frac{\partial u_i}{\partial x_2} = \frac{\partial u_i}{\partial t} + \frac{\partial p}{\partial x_i}, \quad (i = 1, 3), \tag{15}$$

where in a local coordinate system, x_2 indicates the wall-normal direction and $x_i\,(i = 1, 3)$ are tangential to the wall. The mixing-length eddy viscosity model with damping function is adopted to account for the near-wall turbulence

$$\nu_t = \kappa \nu x_2^+ (1 - e^{-x_2^+/A})^2, \tag{16}$$

where $\kappa = 0.4$ and $A = 19$. If the wall-normal velocity is needed like in discrete momentum forcing IB method, it can be obtained from the continuity equation

$$v_2(x_1, x_2, x_3) = -\int_0^{x_2} \left(\frac{\partial u_1}{\partial x_1} + \frac{\partial u_3}{\partial x_3}\right) \mathrm{d}x_2'. \tag{17}$$

The simplified unsteady TBLE without convective terms are treated as ordinary differential equations at each time step. Therefore, they can be integrated from $x_{2o} = \delta$ down to the wall to give a closed-form expression of the wall shear stress components

$$\tau_{wi} = \nu \frac{\partial u_i}{\partial x_2}\Big|_{x_2=0} = \frac{1}{\int_0^\delta \frac{\mathrm{d}x_2}{\nu+\nu_t}} \left\{ u_{oi} - \frac{1}{\rho}\frac{\partial p}{\partial x_i} \int_0^\delta \frac{x_2 \mathrm{d}x_2}{\nu + \nu_t} - \int_0^\delta \frac{\int_0^{x_2} \frac{\partial u_i}{\partial t} \mathrm{d}x_2'}{\nu + \nu_t} \mathrm{d}x_2 \right\}. \tag{18}$$

If the time derivative is eliminated, and if the turbulent viscosity ν_t only depends on the friction velocity and the wall distance, the above equation can be integrated numerically to obtain the final wall shear stress. Otherwise, the velocity distribution in the wall layer has to be computed. We discretize Eq. 15 by a second-order central scheme on a locally defined, one-dimensional stretched grid between the wall and the interpolation point in the wall-normal direction. The no-slip boundary condition is imposed at the wall. The upper boundary conditions for velocity and pressure gradients are interpolated from the exterior LES. This results in a tridiagonal linear equation system that is directly solved using a standard procedure. Note that the TBLE are solved at every Runge-Kutta substep and the velocities on the embedded grids are updated by the same Runge–Kutta method as the LES time derivative term.

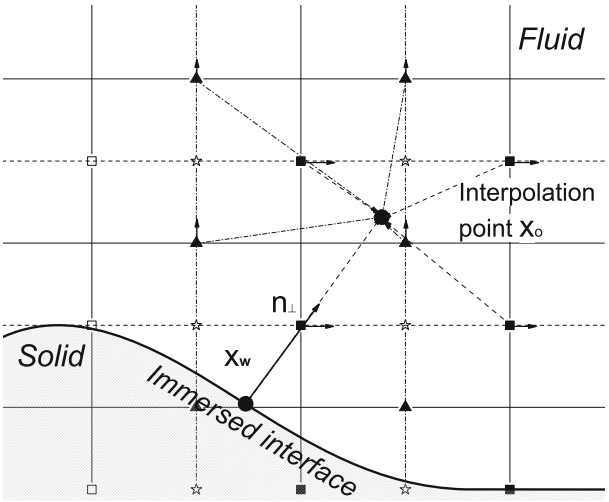

Fig. 2 The sketch of interpolation and tangential direction definition

For body-fitted structured meshes, it is straightforward to define an increased-resolution wall-normal grid for the TBLE and to interpolate velocity and pressure from the LES-grid nodes. Also, it is straightforward to compute the pressure gradient in the wall-parallel directions. The wall stresses computed from the TBLE can be used directly as diffusive wall flux in Eqs. (5). The situation is more complex with immersed-interface methods, because the wall geometry does not conform to the background Cartesian mesh. The local wall-normal and wall-tangential directions have to be defined for each cut cell separately. First, the unit normal vector $\mathbf{n}_\perp$ to the wall is obtained from the gradient of the level-set function. Second, one wall-tangential direction $\mathbf{t}_1$ is defined from the intersection between the plane spanned by the normal vector and one axis of the underlying Cartesian system. Any one of the three unit vectors of the underline Cartesian system can be used, but it should not be chosen along the wall-normal direction. The other wall-tangential direction $\mathbf{t}_3$ is obtained by the cross-product of the wall-normal and the first wall-tangential vectors. Velocity vector and pressure gradient are interpolated from the LES mesh using trilinear interpolation at points away from the wall in the wall-normal direction. Subsequently, they are projected onto the wall-tangential directions to obtain the outer boundary conditions for the TBLE, as sketched in Fig. 2. For imposing wall stresses from TBLE as wall fluxes of the LES, a tensor transformation is necessary to translate them into the stress components in Cartesian coordinates. A simpler equivalent alternative is to compute the wall shear force $\mathbf{f}_w$ from the wall stresses $\tau_{wi}(i = 1, 3)$ and the local wall-surface area $\Gamma_{i,j,k}$ and volume of the cut cell $V_{i,j,k}$, which is then projected onto the Cartesian coordinate system. This can be summarized as

$$\mathbf{f}_w = (f_{wx}, f_{wy}, f_{wz}) = \frac{1}{V_{i,j,k}}(\mathbf{t}_1\tau_{w1} + \mathbf{t}_2\tau_{w2})\Gamma_{i,j,k}, \tag{19}$$

where f_{wx}, f_{wy}, and f_{wz} are the three components of the wall shear force. These projected forces can be used as source terms in the momentum equations Eqs. (5a).

We emphasize that with the present method, only the diffusive flux or wall shear force is provided to the exterior LES. The wall-normal cell-averaged velocity for the cut cell is the solution of the exterior flow LES, Eqs. (5, 9), and not directly affected by the wall model. The impermeability condition is imposed by Dirichlet boundary conditions on the convective interface interaction, that is, $\mathbf{C}_{\Gamma_{i,j,k}} = 0$ for non-moving walls, and a homogeneous Neumann boundary condition for the pressure that is directly implemented in the pressure Poisson solver. This is an important difference from immersed-boundary methods that are based on the discrete momentum forcing at the first off-wall grid point. As the first off-wall grid point never coincides with the immersed wall boundary, the wall-normal velocity needs to be reconstructed in discrete-forcing methods and then projected onto the Cartesian coordinate system to evaluate the forcing term. The present cut cell method is not only fully conservative but also expected to be more robust than the discrete momentum forcing immersed-boundary method, in particular if high-order discretization schemes are used.

Table 1 Simulation cases and resolutions

Case	Re_τ	$N_{x_1} \times N_{x_2} \times N_{x_3}$	N_{TBLE}
wm_1	395	$16 \times 16 \times 16$	20
wm_2	590	$16 \times 16 \times 16$	20
wm_3	950	$16 \times 16 \times 16$	20
wm_4	2,000	$16 \times 16 \times 16$	20
wm_5	25,000	$32 \times 32 \times 32$	40
wm_6	100,000	$48 \times 48 \times 48$	40
wm_7	100,000	$32 \times 32 \times 32$	40
wm_8	2,000; 25,000; 100,000	$48 \times 48 \times 48$	40

4 Assessment of wall model with implicit LES

In this section, the performance of the wall model in conjunction with the implicit LES model is investigated in detail for turbulent channel flow. An initial test of the further extension to a wall model with implicit LES and immersed-interface method is also performed, where the channel walls are moved off the computational grid.

We consider the same setup for the turbulent channel flow with $\Delta_0 = L_0/32$ and $L_0 = 2H/3$ in Eq. (7) as in Ref. [24], where H is the half channel height. The computational domain size is $2\pi H \times 2H \times \pi H$ in the streamwise, the wall-normal, and in the spanwise directions, respectively. The grid resolutions for the LES and the local embedded TBLE are shown in Table 1 and denoted as $N_{x_1} \times N_{x_2} \times N_{x_3}$ and N_{TBLE}, respectively. The grid spacing is uniform in each coordinate direction in the LES domain and it is stretched in wall-normal direction in the TBLE domain. The coupling position x_2 is at the first off-wall grid point of the LES mesh, except for case wm_1, where it is centered between the first and second grid points in the lower part of the logarithmic layer. Periodic boundary conditions are used in the streamwise and in the spanwise directions.

Results for the mean velocity, non-dimensionalized by wall units $l^+ = \nu/u_\tau$ and friction velocity u_τ, are compared with direct numerical simulations (DNS) and the logarithmic law in Fig. 3. At moderately large Re_τ, the mean-velocity profiles are predicted well. However, at very large $Re_\tau = 25{,}000$ and $Re_\tau = 100{,}000$, the mean velocities exhibit a logarithmic-layer mismatch [9]. From inspecting the results, we find that the damping function Eq. (8), which was developed for wall-resolving LES, has a relevant effect only on the wall cells with very weak parameter dependence [24]. In conjunction with the TBLE-based wall model, this results in an underprediction of wall stresses at large Reynolds numbers. At these large Reynolds numbers, the near-wall LES-grid cells are very large in terms of viscous length scales l^+, and the damping function Eq. (8) ceases to be physically meaningful. It can be expected that a physically meaningful damping function to be used in conjunction with wall models may remedy the problem. We found that an adaptive coefficient formulation based on the findings of Ref. [33] is suitable for this purpose. In the following, we refer to this modification as coherent structures (CS) damping, details are given in the Appendix. As with the CS modification, the SGS model dissipation is too small in the wall cells, we copy $\boldsymbol{\sigma}_{i,j,k}$ of Eq. (7) for these cells from the next neighbors away from the wall. With this fix, the resulting mean-velocity profiles and Reynolds stresses are predicted as well as for the original formulation at moderately large Re_τ, see Figs. 3 and 4, but now are significantly improved for large Re_τ, as shown in Fig. 3 for $Re_\tau = 25{,}000$ and $Re_\tau = 100{,}000$.

The von Kármán constant appears to be slightly underpredicted by the results of Fig. 3 at $Re_\tau = 100{,}000$, which can be attributed to the fact that at the coupling position of $x_2^+ = 2{,}230$, convective effects probably are so strong that they contribute to the near-wall behavior while being neglected in the TBLE. Without increasing the grid resolution, the coupling point can be moved closer to the wall by employing a stretched grid in the wall-normal direction, for example, mapped by a hyperbolic tangent function

$$x_{2j} = -\frac{H}{\tan h(C_G)} \tan h\left(C_G - 2C_G \frac{j}{N_{x_2}}\right), \tag{20}$$

with $C_G = 1.5$. With the same grid resolution as case wm_7 in Table 1, the coupling position is now at about $x_2^+ = 1,000$. The mean-velocity profiles are compared in Fig. 5. One can see that with the original formulation for $\boldsymbol{\sigma}_{i,j,k}$, the predicted mean velocity deteriorates with grid stretching as in this case the overestimated value of $\boldsymbol{\sigma}_{i,j,k}$ in the near-wall cells becomes even larger. The CS modification is found to behave well and exhibits only weak grid size dependence. From the comparison of the streamwise shear stress balance in Fig. 6, one can see that the resolved shear stress becomes larger near the wall and that the modeled subgrid stress becomes

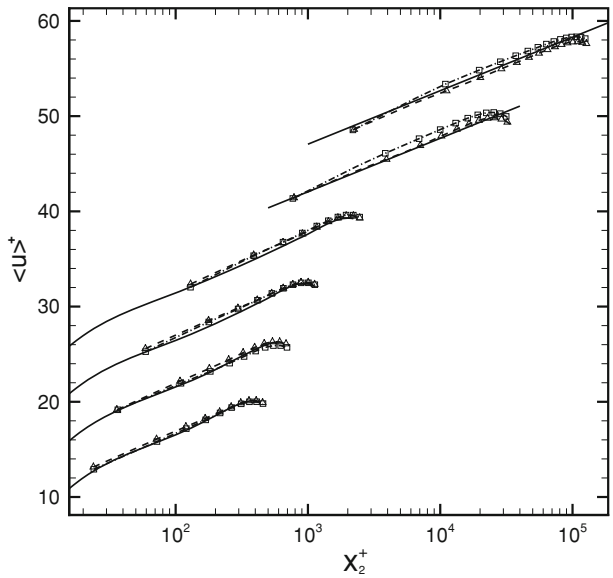

Fig. 3 Mean velocity comparisons of cases wm_i, $(i = 1 \sim 6)$ from bottom to top, the velocity profiles are shifted upward by $(i - 1)5$ for clarity. *The solid lines* from bottom to top DNS at $Re_\tau = 395$ [38], $Re_\tau = 590$ [38], $Re_\tau = 950$ [2], $Re_\tau = 2{,}000$ [28] and the last *two* $2.44\ln(x_2^+) + 5.2$; *dashdot lines with square* VD; *dashed lines with delta* CS

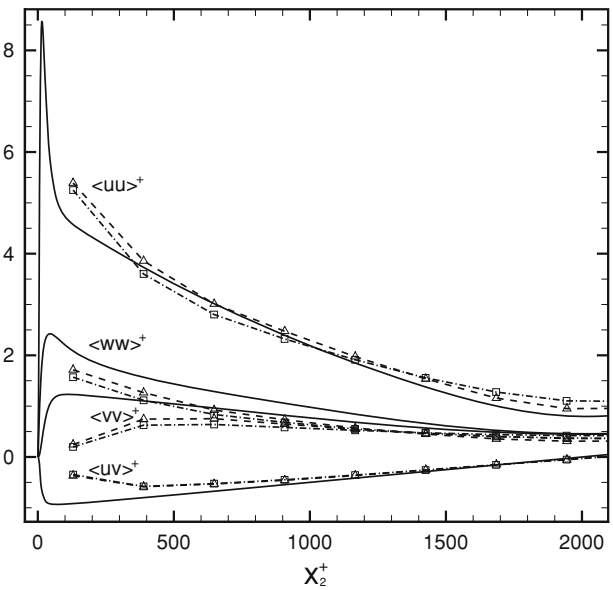

Fig. 4 Reynolds stresses comparisons of case wm_4. *The solid line* DNS [28]; *dashdot lines with square* VD; *dashed lines with delta* CS

smaller, while the viscous stress remains almost the same when CS is used. This trend confirms the fact that mean-velocity artifacts are caused by the overpredicted subgrid stress at several near-wall grid points.

To better assess the effect of the TBLE turbulence model on the dynamics of the wall layer, three different eddy viscosity RANS models are investigated for case wm_4 in Table 1. The first eddy viscosity model, denoted as M1, is our standard formulation from Eq. (16). As M2, we denote the Baldwin–Lomax model [7] which uses a two-layer formulation. The inner layer is based on the friction velocity scale and the outer layer is based on the velocity scale deduced from the resolved vorticity. The last model is the formulation of Balaras et al. [6] denoted as M3

$$\nu_t = (\kappa y)^2 |\overline{\mathbf{S}}| D, \quad D = [1 - \exp(-(y^+/A)^3)], \tag{21}$$

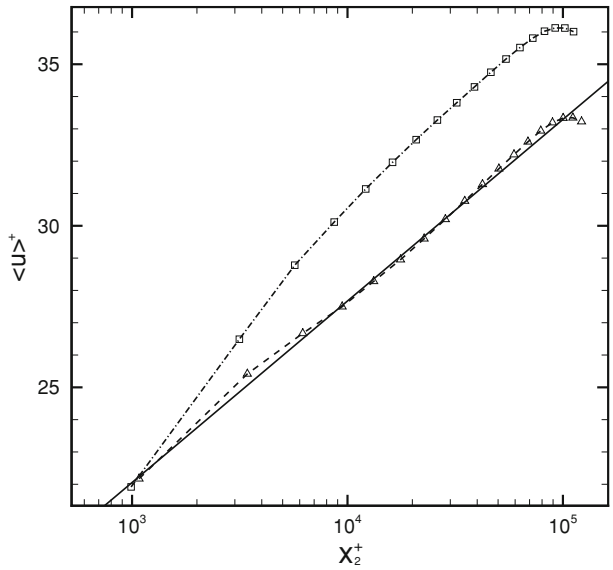

Fig. 5 The grid stretching effect on the mean velocity of case wm_7. *The solid line* $2.44ln(x_2^+) + 5.2$; *dashdot line with square* VD; *dashed line with delta* CS

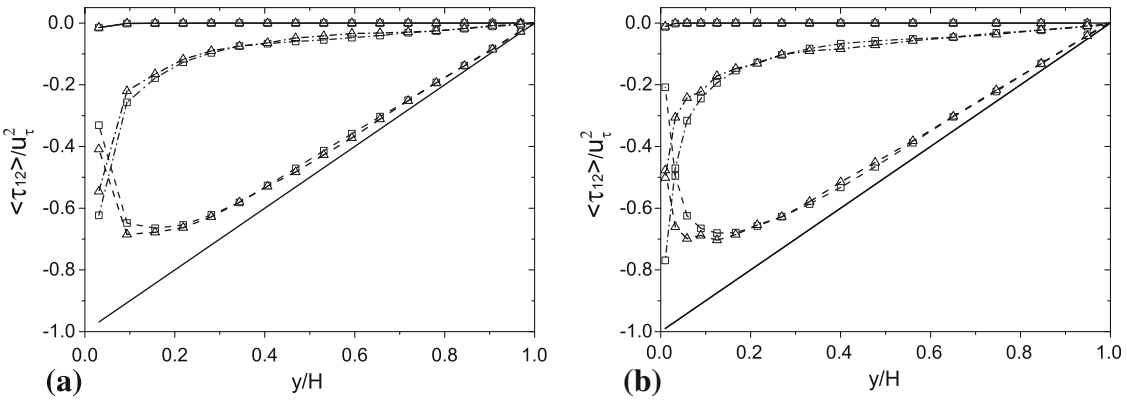

Fig. 6 Streamwise shear stresses balance comparison using VD and CS. *Solid lines with symbols* viscous stress; *dashed lines with symbols* resolved shear stress; *dashdotted lines with symbols* SGS shear stress; *solid line* total shear stress. *Lines with square* VD; *lines with delta* CS. **a** Case wm_5, **b** case wm_7 with wall-normal grids stretched

where $|\bar{\mathbf{S}}|$ is the magnitude of the resolved strain at the coupling position, providing the velocity scale, and $A = 25$.

The comparisons of the mean-velocity profiles of inner TBLE and exterior LES are shown in Fig. 7a. The mean velocity of the TBLE region is best predicted by M1. M3 underpredicts the wall shear stress and gives poor results for the buffer region. M2 yields almost the same wall shear stress as M1, although the prediction for outer part of TBLE region is slightly worse. From the comparison of the local von Kármán constant $\kappa = \frac{1}{y^+ d\bar{u}^+/dy^+}$ in Fig. 7b, it can be seen that all TBLE turbulence models result in almost identical predictions for logarithmic region in the exterior LES. This is confirmed in Fig. 8 by the resolved shear stress and the non-dimensionalized turbulence production. The Reynolds shear stress is plotted in Fig. 8a. M2 and M3 produce a modeled Reynolds shear stress that approaches the resolved Reynolds shear stress of the LES at the coupling position. This due to the fact that M2 and M3 use velocity scales in the eddy viscosity formulation that is based on the resolved strain and vorticity of the exterior LES. With M1, we observe a discontinuity between the RANS modeled Reynolds stress in the TBLE region and the resolved Reynolds stress in the LES domain. From the continuous derivative of the mean-velocity profile, see Fig 7a, we can deduce that this discontinuity properly reflects the differences in modeling approaches of TBLE and LES, in particular the contribution of the implicitly modeled SGS stress in the LES region. Note that only M1 yields a smooth velocity profile without a

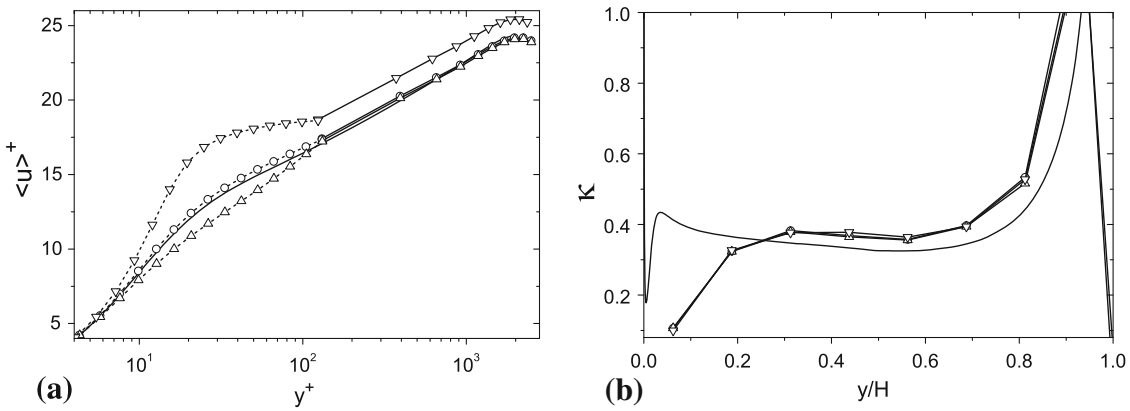

Fig. 7 Effect of eddy viscosity model on mean velocity and κ of coarse LES with TBLE model at $Re_\tau = 2{,}000$. *Solid lines* DNS; *Solid lines with symbols* exterior LES; *Dashed lines with symbols* inner TBLE. *Circle* M1—present model, see Eq. (16); *uptriangle* M2—Baldwin-Lomax model [7]; *downtriangle* M3—Balaras et al. [6]. **a** Mean-velocity profiles, **b** local von Kármán constant κ

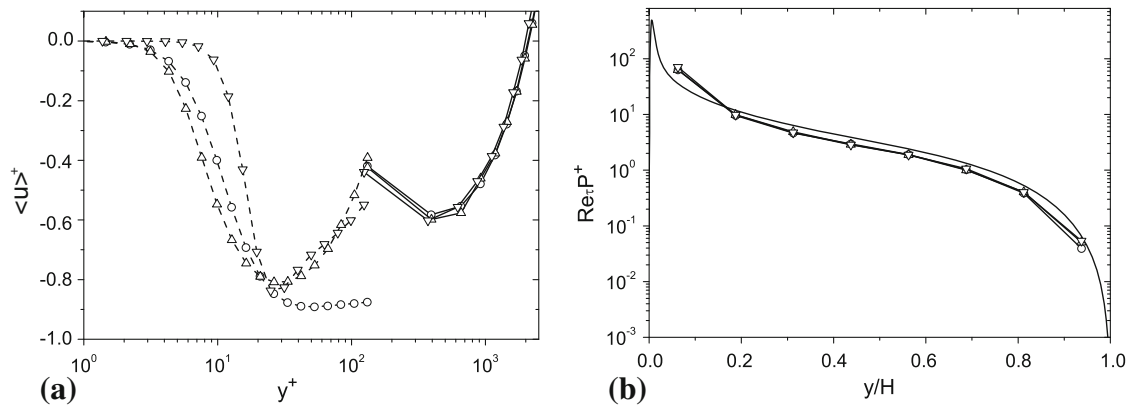

Fig. 8 Effect of eddy viscosity model on Reynolds shear stress and turbulence production for coarse LES with TBLE model at $Re_\tau = 2{,}000$. *Lines* labeled as in Fig. 7. **a** Reynolds shear stress, **b** turbulence production

log-layer mismatch between TBLE and LES domain. The above analysis indicates that a key issue for a wall model is to provide the correct wall shear stress, and that the exterior LES is not very sensitive to the details of near-wall turbulence modeling.

The grid resolution of the exterior LES is also investigated. Although a grid convergence study cannot be carried out as with traditional RANS, we can assess whether the prediction of the resolved part of the flow improves with increasing grid resolution with the wall model being active. Three cases at $Re_\tau = 2{,}000$ using different resolutions $16 \times 16 \times 16$, $32 \times 32 \times 32$, and $48 \times 48 \times 48$ are denoted as $R1$, $R2$, and $R3$, respectively. All the grids are equidistant.

The results for mean velocity and local von Kármán constant κ are compared in Fig. 9a, b, respectively. As the resolution increases, the first off-wall point approaches the wall, but it is still outside of the buffer layer. The well-established logarithmic regions extend toward the wall and leave the outer part unchanged, which is indicated clearly by the local κ in Fig. 9b. It can also be observed that κ is not exactly constant with increasing resolution, but approaches the DNS result. The resolved turbulence production also approaches that of DNS, as shown in Fig. 9c, while there still remains a small deficit at the finest resolution in the outer part. A similar observation can be made for the different shear stresses (resolved, molecular, and modeled subgrid stress), as shown in Fig. 9d. From the above results, we can see that as long as the constraint of the wall model with respect to the coupling position is satisfied, consistent results can be obtained when the grid resolution varies.

As our main intention is to use TBLE wall modeling in conjunction with implicit LES and an immersed-interface method for complex geometries, it is sensible to test this combination first for a very simple configuration. For the turbulent channel flow, case wm_8 of Table 1, we immerse the plane channel of domain size $2\pi H \times 2H \times \pi H$ into a computational domain of size $2\pi H \times 2.35H \times \pi H$, which is discretized by

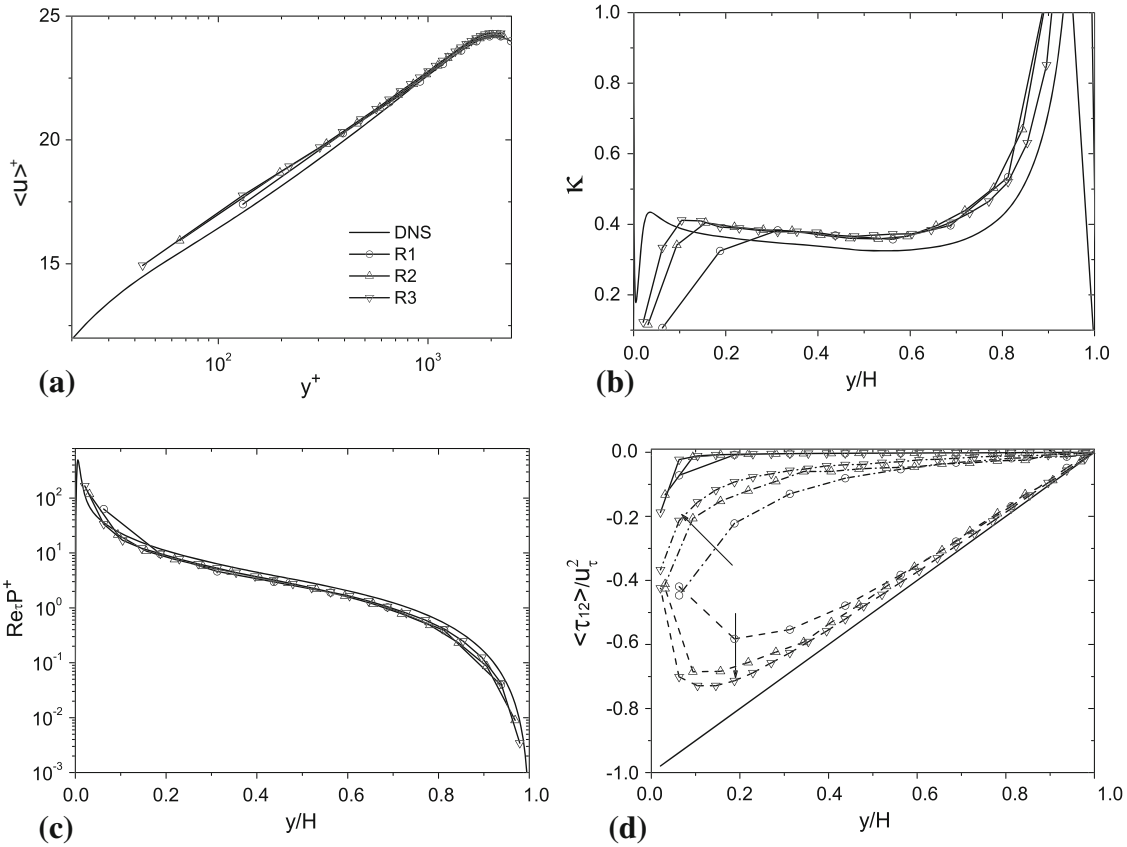

Fig. 9 Effect of resolution of exterior LES on mean velocity, local κ, turbulence production, and shear stress balance for coarse LES with TBLE model at $Re_\tau = 2{,}000$. In (**d**), line styles denote different stresses as in Fig. 6. *Arrows* point to the direction increasing resolution. **a** Mean streamwise velocity, **b** local von Kármán constant κ, **c** turbulence production, **d** streamwise shear stress balance

$48 \times 48 \times 48$ regular cells in three directions. Periodic boundary conditions are applied in the streamwise and the spanwise directions, and the wall model is used at both immersed interfaces. The coupling points between TBLE and LES grid are placed one wall-normal grid spacing away from the interfaces. The wall model with CS damping is used. Results for mean velocities and Reynolds stresses are shown in Figs. 10 and 11, respectively. The mean velocities are predicted with similar accuracy as for the wall-conforming boundary, compare with Fig. 3. The prediction of the Reynolds stresses is also of similar quality as for the wall-conforming case, compared with Fig. 4. The oscillation over the first few grid points is caused by the momentum-mixing procedure of the immersed-interface method, see Ref. [35], which for the severe setup chosen above occurs for each wall cell.

From the results presented in this section, we can come to the following conclusions. First, the original version of ALDM, extended by a simplified TBLE-based wall model gives good results for turbulent channel flow up to moderately large Reynolds numbers. At very large Reynolds numbers, a logarithmic-layer mismatch occurs due to overestimated SGS dissipation in the near-wall cells. Nevertheless, the observed effect is weaker than that of Ref. [13,39] using explicit eddy viscosity models. A significant improvement for the wall model is achieved by introducing a physically meaningful damping function by CS. Artifacts at large Reynolds numbers can be almost entirely removed. Second, ALDM and wall model work properly in conjunction with the CIIM.

5 Application of the wall model, ALDM, and CIIM to backward-facing step flow

To test the full approach for a moderately complex geometry, we consider the flow along a backward-facing step at $Re_h = 5{,}000$ according to the experiment of Jovic and Driver [31] as reference. Compared to the turbulent channel flow, additional complications are introduced with respect to wall model formulation and flow dynamics. With respect to the former, the wall-normal direction is not continuous and jumps at the corners,

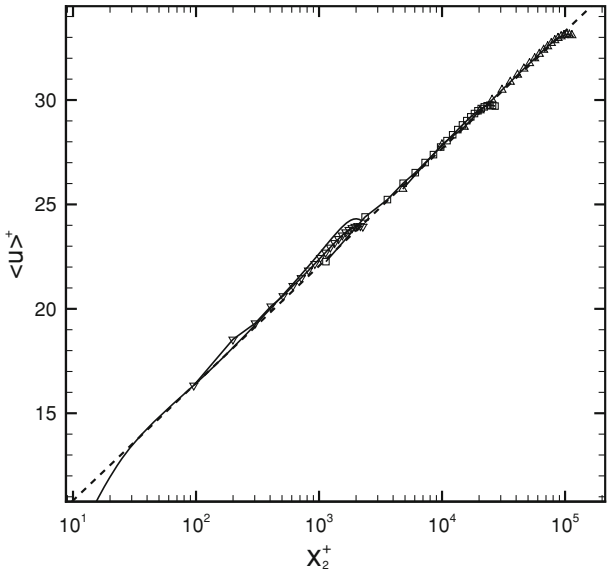

Fig. 10 The mean velocity comparison of case wm_8 with DNS and logarithmic law. *The solid line* DNS at $Re_\tau = 2{,}000$ [28]; *dashed line* $2.44\ln(x_2^+) + 5.2$; *solid line with nabla* $Re_\tau = 2{,}000$; *solid line with square* $Re_\tau = 25{,}000$; *solid line with delta* $Re_\tau = 100{,}000$

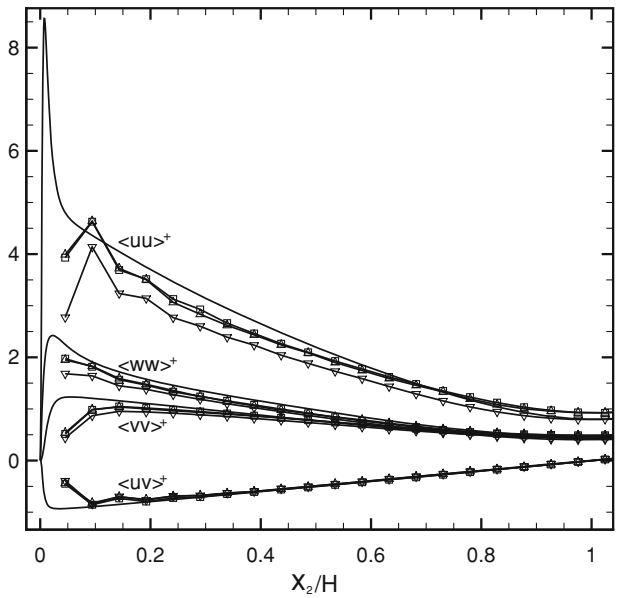

Fig. 11 Reynolds stresses comparisons of case wm_8 with DNS at $Re_\tau = 2{,}000$. The *lines* labeled as in Fig. 10

which poses a difficulty for the underlying level-set representation of the wall and for defining unambiguously the wall-tangential directions. With respect to the latter, the flow now includes a separation, a separated shear layer, a recirculation bubble formation, flow reattachment, and recovery. The considered computational domain extends in streamwise direction for $40h$, where h is the step height, including a section of $10h$ upstream of the step. The height is $6h$ at the outlet, the spanwise width is $3h$, and an expansion ratio is 1.2. A multiblock boundary-conforming grid and the CIIM method are used for comparison.

For the boundary-conforming computation, the flow domain is divided into three blocks at the step, which are discretized by $192 \times 32 \times 24$ cells, with 48 cells upstream of the step. In the streamwise direction, the grids are refined near the location of the step. A recycling inflow technique [26] and a convective outflow boundary condition are applied in the streamwise direction. A symmetry boundary condition is used at the upper boundary. A periodic condition is used in the spanwise direction. At the wall, alternatively, a no-slip

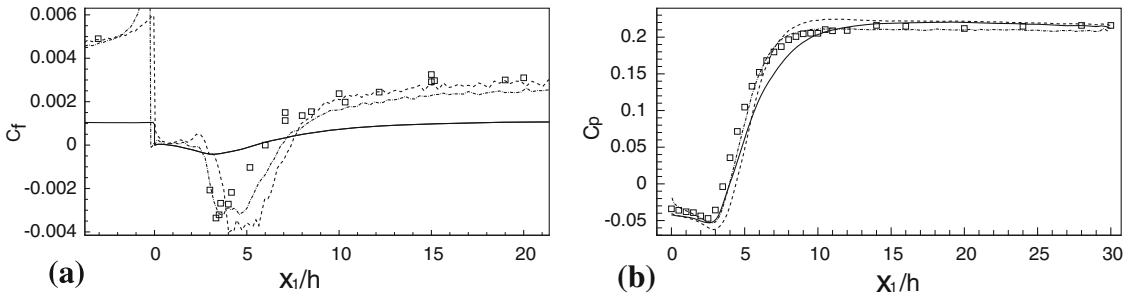

Fig. 12 Comparisons of friction and pressure coefficients. *Square symbols* experiment; *solid line* LES_CS; *dashed line* WM_CS; *dashdot line* WM_IB. **a** Friction coefficient, **b** pressure coefficient

condition (LES resolution not resolving the near-wall flow) and the above wall model are used. These cases are distinguished as LES_CS and WM_CS, respectively.

For the CIIM computation, the computational domain size is $40h \times 6.5h \times 3h$ in the streamwise, vertical, and spanwise directions, respectively. The step is immersed into the computational domain and does not collapse with computational grid lines. The resolution is $192 \times 44 \times 24$ and is comparable with the boundary-conforming case using the same grid refinement near the step. The same boundary conditions as for the boundary-conforming case are used, except for the wall boundaries, where the wall stresses from the wall model are imposed by CIIM. This case is denoted as WM_IB.

In all cases, the pressure Poisson equation is solved using a fast Fourier transform in the spanwise direction, and a two-dimensional BiCGStab iterative solver for the other directions. The resolution of the locally embedded TBLE grid is 20 for all cases. The coupling position is about $x_2^+ = 50$, based on the local friction velocity at inlet. As the friction Reynolds number is comparably low, we cannot distinguish results of the original VD and the CS modification, as the case for the turbulent channel flow. Therefore, only the results obtained with the CS modification are presented.

The reattachment length x_r/h of LES_CS, WM_CS, and WM_IB are 5.4, 7.4, and 6.85, respectively, as indicated by the location of zero mean friction coefficient in Fig. 12a. If the 50 % forward-flow criterion at the first off-wall points is used to identify reattachment, x_r/h becomes 5.4, 5.8, and 5.2, respectively. For the LES_CS case, these points obviously are in the LES region, whereas for the two other cases, these points are the first off-wall points of the TBLE. This difference is partially responsible for the rather large discrepancy between the coarse-resolved LES and the wall model results. The computed reattachment lengths are all quite different from that of the experiment $x_r/h = 6.0 \pm 0.15$, as they strongly depend on the boundary layer upstream of the step and on the effective dissipation in the recirculation region. For the LES without wall model, LES_CS, the boundary layer upstream of the step is not predicted correctly due to the coarse resolution. For the cases with wall modeling, although the outer part of incoming boundary layer is more accurate (see below), the wall model is insufficient for an accurate prediction of the recirculation region. The DNS of Le et al. [34] shows that a second recirculation occurs at the lower corner of the step and has a length $1.76h$ and a height $0.8h$. For the wall-modeling cases, WM_CS and WM_IB, the main recirculation bubble extends all the way to the step and no secondary separation bubble is observed, a behavior which has been reported in Ref. [12] for all kinds of wall model used in this reference and also for a coarse LES without wall model. It should be pointed out that for our coarse-resolved LES_CS with ALDM, a secondary recirculation bubble of size $0.75h \times 0.7h$ is observed. This observation supports our conclusion that the occurrence of the secondary recirculation bubble rather depends on the SGS model quality than on near-wall grid resolution. We also support the observation that TBLE-based wall modeling is unable to recover such effects.

The friction- and pressure-coefficient distributions

$$C_f = \frac{\tau_w}{\frac{1}{2}\rho U_0^2}, \quad C_p = \frac{p - p_0}{\frac{1}{2}\rho U_0^2}, \tag{22}$$

are compared in Fig. 12, where p_0 is the reference pressure taken at $x_1/h = 5.1$ upstream of the step. U_0 is the upstream reference velocity at $x_1/h = 3.05$, defined following the experiment, which is also used to non-dimensionalize the mean velocity and Reynolds stresses. From the C_f distribution, it can be seen that C_f is strongly underpredicted in LES_CS, as expected. Upstream of the step, the boundary layer develops under the influence of a weak favorable pressure gradient and the C_f is predicted well by the wall models.

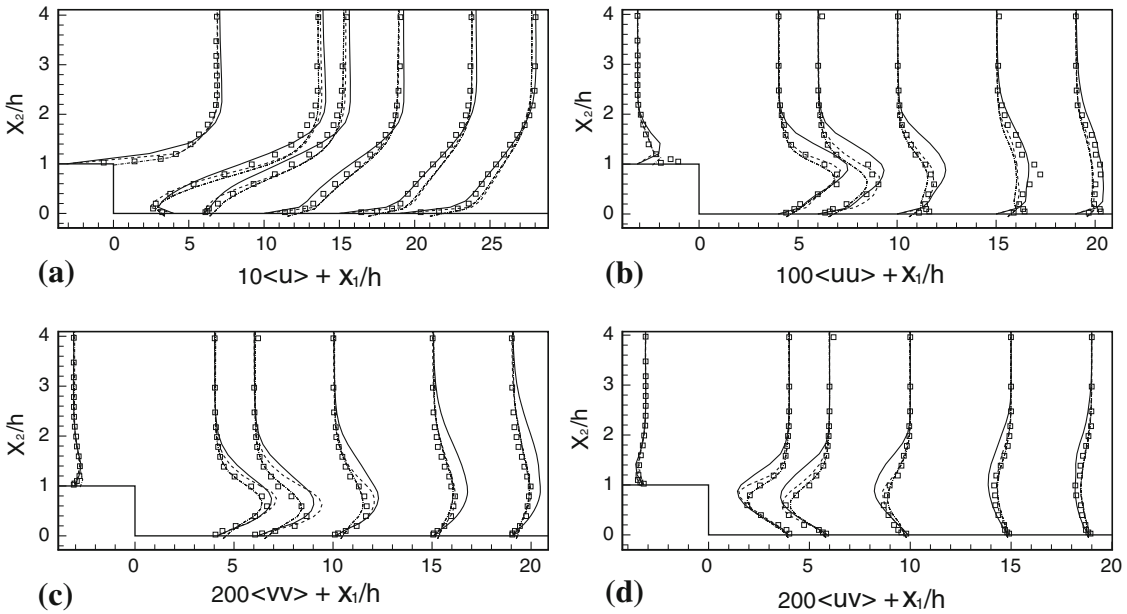

Fig. 13 Comparisons of mean velocity and Reynolds stresses at six stations. *Lines* labeled as in Fig. 12. **a** Mean streamwise velocity, **b** longitudinal Reynolds normal stress, **c** transverse Reynolds normal stress, **d** Reynolds shear stress

In the recirculation region, the wall model fails to recover the correct C_f. In the front part of the recirculation, a weak favorable pressure gradient causes the wall friction to become positive for WM_CS. In the rear part of the recirculation, the overpredicted adverse pressure gradient results in a negative C_f farther downstream than for the experiment. We conclude that the wall friction is dominated by the pressure gradient through the simplified TBLE, and the prediction deficiencies may be related to the neglected convection terms.

In the recovery region, C_f is predicted well by WM_CS, while being underpredicted in WM_IB. The absolute values of C_f from WM_IB are smaller than those from WM_CS, except near the upstream of the step. As can be seen from the C_p distribution, the pressure recovers more quickly in the wall-modeling cases than for LES_CS. For WM_CS, the pressure is lower than that of LES_CS in the rear part of the recirculation, which indicates a stronger recirculation in WM_CS. However, downstream of the position $x_1/h = 14$, the pressure coefficients are almost the same in both cases. With WM_IB, the pressure is overpredicted near the step, a behavior that is caused by the cut cells at the upper and lower corners. In the recovery region, the pressure coefficient is predicted well, where the momentum-mixing results in a larger near-wall velocity and thus a lower pressure.

The streamwise mean-velocity and Reynolds-stress profiles are shown in Fig. 13a–d at six downstream stations. Upstream of the step, at station $x_1/h = -3.1$, the flow resembles a developed turbulent boundary layer with a weak favorable pressure gradient. For the wall-modeling cases, the mean velocities and Reynolds stresses are predicted well outside of the wall layer at this station. However, for LES_CS, the mean velocity is underpredicted near the wall and overpredicted away from the wall. The position of the maximum streamwise Reynolds normal stress is shifted further away from the wall. The other Reynolds stresses are predicted well. At the location $x_1/h = 4.0$, the maximum mean backflow velocity is underpredicted for LES_CS and for WM_IB, which is consistent with the too short reattachment length.

In the wall-modeling cases, the coupling positions are approximately at the locations of the maximum backflow velocity. Beneath those locations, the turbulence production in the real flow is very small [1]. The mixing-length eddy viscosity model, however, introduces a rather strong turbulence production in the TBLE and fails to recover this kind of flow. At reattachment and further downstream, the prediction of mean velocities and Reynolds stresses is generally improved by the wall model, except at the far-downstream stations. It can be seen that for the wall-modeling simulations, the flow recovers too quickly after the reattachment, as shown in Fig. 13a. In the rear part of the recovery region, although the pressure gradient is almost zero, the boundary layer is far from well-developed [31,34]. A inner boundary layer occurs near the wall, and the outer flow is still affected by the evolution of the free shear layer that has experienced a strong adverse pressure gradient. The mixing length and the eddy viscosity are much larger than the ones obtained from using Eq. (16) with

Table 2 Simulation parameters of the periodic hill

Case	Re_H	$N_{x_1} \times N_{x_2} \times N_{x_3}$	CFL	T_{avg}	x_{sep}/H	x_{reatt}/H
LES_C	10,595	$96 \times 64 \times 32$	0.25	90	0.52	3.15
$WMLES\_C$	10,595	$96 \times 64 \times 32$	0.25	90	0.65	4.00
$WMLES\_F$	10,595	$192 \times 72 \times 64$	0.25	40	0.50	4.42
$WMLES\_C37$	37,000	$96 \times 64 \times 32$	0.5	90	0.75	3.41
$WMLES\_F37$	37,000	$192 \times 72 \times 48$	0.5	40	0.75	3.80

$\kappa = 0.4$ [30]. This fact results in an underprediction of the wall stresses by TBLE, as in Fig. 12a. Thus, the flow recovers too fast with an overpredicted mean velocity. For WM_IB, the transverse Reynolds normal stress and Reynolds shear stress are in better agreement with the experiment than those of WM_CS. This can be attributed to the favorable effect of artificial momentum mixing near the wall, which is consistent with the more accurately predicted pressure coefficient. Note that again we have chosen a worst-case scenario for positioning the lower wall with respect to the computational grid. The chosen position leads to the situation that momentum mixing is applied all along the lower wall downstream of the step.

From the above analysis, we conclude that even the simple TBLE wall model used here generally improves the prediction of the mean flow. On the other hand, it may prevent the evolution of small-scale near-wall flow structures such as the secondary separation for the backward-facing step flow. We also have observed that CIIM with wall model occasionally may lead to a fortuitous situation where the mixing rule employed for relaxing the numerical stability constraint in CIIM interacts favorably with the wall model.

6 Application of the wall model, ALDM, and CIIM to channel flow with periodic constrictions

We consider the flow over periodic hills in a channel as investigated, e.g., by Fröhlich et al. [18] and Breuer et al. [11]. The flow is characterized by separation from the smooth curved surface, recirculation area, reattachment at the flat plate, and acceleration on the windward side of the hill. Most statistical turbulence models have difficulties to predict these flow features or even the separation length. A simulation with highly resolved LES on the hill side and wall modeling on the straight side was carried out by Fröhlich et al. [18], investigating the physical issues of this test case comprehensively at $Re_H = 10{,}595$. Wall-modeling issues were extensively investigated combining different SGS models with different wall models on the coarse body-fitted grids [47], which highlighted the importance of an adequate streamwise resolution of the flow in the vicinity of the separation line. The near-wall treatment was found to have more effect than the SGS model on the quality of the results obtained on coarse grids. It should be mentioned that an alternative modeling strategy for separated flows has been proposed by Breuer et al. [11] using statistical evaluations of wall-resolved LES data. Also, hybrid LES/RANS approaches including detached-eddy simulation (DES) have been evaluated on this test case, see, e.g., [10,49], where a massive deterioration of the results was detected when the LES/RANS interface moves outside of the boundary layer on the crest of the hill.

The overall simulation domain is $9.0H \times 3.335H \times 4.5H$. Periodic conditions are used in the streamwise and spanwise directions, and wall models are adopted at the immersed interfaces representing the hill. Based on the results for the backward-facing step, a coarse resolution of $96 \times 64 \times 32$ cells in the streamwise, vertical, and spanwise directions is used for coarse LES with and without wall modeling. A fine resolution of $192 \times 72 \times 64$ is also used to investigate the effect of grid resolution. The computational parameters are shown in Table 2 for detail, where the streamwise separation and reattachment positions indicated by the streamline normal to the wall are also given. Although it is not reasonable to deduce these positions using non-body-fitted coarse Cartesian meshes, it can be seen that the reattachment position is delayed when the wall model or finer resolution is used. Statistics are sampled for about 90 and 40 flow-through times in coarse and fine cases, respectively. Non-dimensional wall distances (based on the friction velocity from resolved LES of Fröhlich et al. [18]) of the matching points between the LES and TBLE domains are about 30 on average, with a maximum of 135.8 at $x_1/H = 8.66$, as shown in Fig. 14 for case $WMLES\_C$. This distance is of half values for case $WMLES\_F$.

The friction and pressure coefficients are compared with those of Fröhlich et al. [18] in Fig 15a, b, respectively. In case LES_C without wall modeling, the wall shear stress far from the resolved values except in the former part of recirculation region from $x_1/H = 0.52$ to $x_1/H = 2.0$. In case $WMLES\_C$, the TBLE-based wall model reproduces reasonably well the overall evolution of the friction coefficient, while showing too low values under adverse pressure gradient conditions. This result is similar to what has been observed for

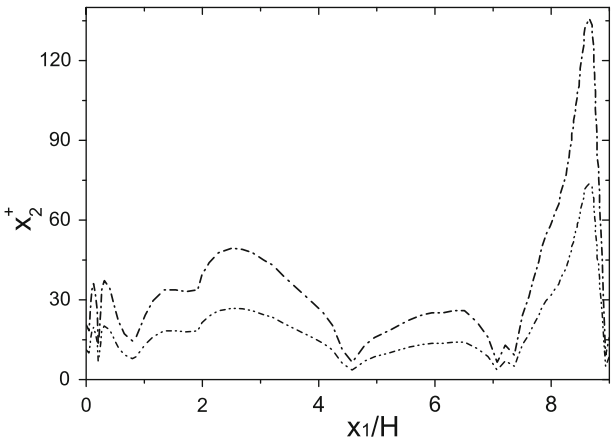

Fig. 14 Non-dimensional wall distance of LES/TBLE matching points on coarse resolutions for the periodic hill on the lower wall at $Re_H = 10{,}595$. *Dashdotted line* $WMLES\_C$; *dashdotdotted line* $WMLES\_F$

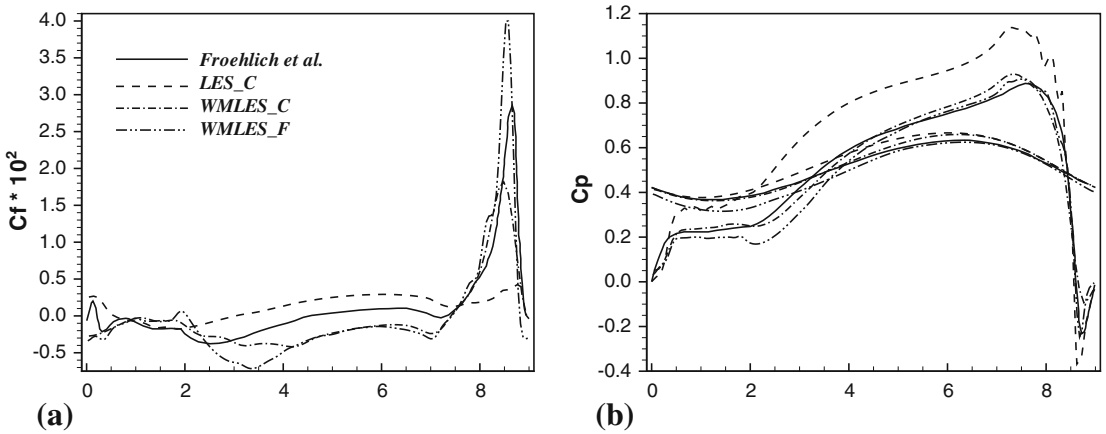

Fig. 15 Comparisons of skin-friction and pressure coefficients for the periodic hill at $Re_H = 10{,}595$. **a** Skin-friction coefficient on the hill, **b** pressure coefficient, the more shallow curve is for the upper wall

the backward-facing step case. This is another indication for the lack of convective effects in the simplified TBLE wall model. In the finer resolution case $WMLES\_F$, for the recirculation becomes larger and stronger than in the coarser case $WMLES\_C$, a smaller negative wall shear stress is produced at the back part of the recirculation. In the recovery region, the wall shear stress is almost the same in these two cases, while in the reacceleration region, the wall shear stress is heavily overpredicted in finer case $WMLES\_F$ due to its large favorable pressure gradient as shown in Fig. 15b.

The pressure coefficient is heavily overpredicted on the hill in case LES_C, but it is reasonable at the upper wall for all cases. On the lower wall, the pressure coefficient indicates that the flow recovers more quickly than the resolved LES in the wall-modeled cases, and the maximum pressure is slightly overpredicted. In the recirculation region, the pressure is lower in case $WMLES\_F$ than in case $WMLES\_C$, which is consistent with the smaller wall friction and stronger recirculation in the former case. Note that a low pressure region on the top of the hill is accompanied by a short closed separation region that cannot be observed in the wall-modeling LES due to the coarse grid resolution, but can be observed in the solution of TBLE.

The mean velocity, turbulent kinetic energy, and Reynolds shear stress are compared with the results of highly resolved boundary-conforming LES using LESOCC [43] at ten sections in Fig. 16. The mean streamwise velocity is overpredicted near the lower wall but it is underpredicted in the upper part of the channel in case LES_C due to the constant mass flux. The vertical mean velocity also has large discrepancies in the recirculation and reacceleration regions, while it is of reasonable values in the recovery region. In wall-modeled cases, the mean streamwise and vertical velocities agree well with resolved LES. But when the grid resolution increases, the streamwise mean velocity has large negative values in the recirculation region,

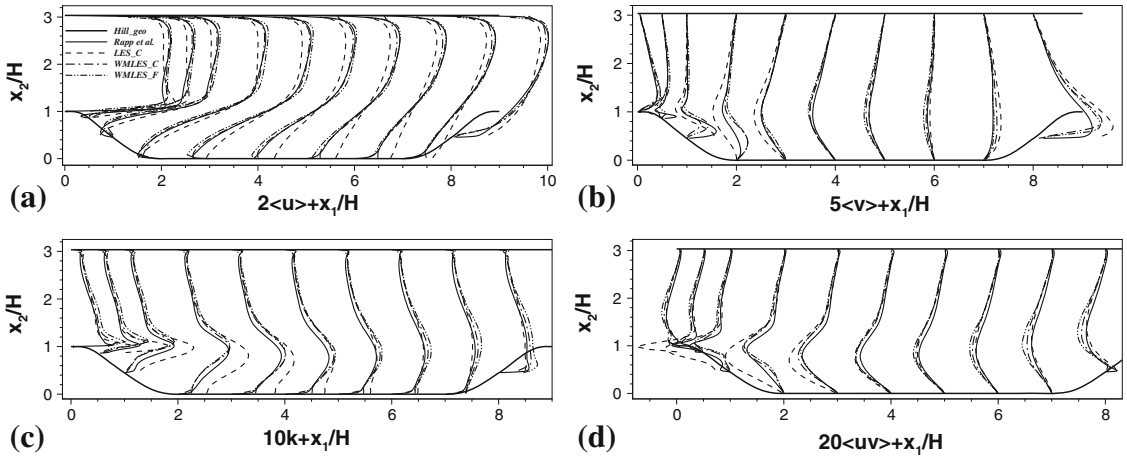

Fig. 16 Comparison of mean-flow variables for periodic hill at $Re_H = 10{,}595$, *lines* labeled as in **a**. **a** Mean streamwise velocity, **b** mean vertical velocity, **c** turbulent kinetic energy, **d** Reynolds shear stress

which causes the streamwise mean velocity upper the recirculation overpredicted. In other attached regions, the mean velocity is improved in finer case, especially near the wall. Largest discrepancies can be observed for the mean vertical velocities, in particular at $x_1/H = 8.0$ in wall-modeled cases, although the pressure gradient is favorable and the non-dimensional wall distance of the LES/TBLE matching point is reasonable as shown in Fig. 14. The reason for this discrepancy is that the boundary layer at this position is strongly unsteady and exhibits a "splatting" phenomenon of large-scale eddies [18]. The turbulent kinetic energy and Reynolds shear stress are heavily overpredicted in the recirculation region for case LES_C as in the backward-facing step. They are reasonably well predicted in the wall-modeled cases. When the resolution increases, there is no obvious improvement, even some larger discrepancies can be observed in the reacceleration region, which can be attributed to the deficiencies of the wall model.

For an assessment of the grid dependence of LES with wall model, additional simulations at $Re_H = 37{,}000$ have been carried out using two resolutions as shown in Table 2. Statistics have been collected for about 90 and 40 flow-through times for the coarse and fine resolutions, respectively. It can also be observed that the reattachment position is delayed in case $WMLES\_F37$ using the fine resolution, while the separation position does not change. Results for the mean velocity and the Reynolds stresses are compared with that of resolved LES using MGLET [43] at ten sections in Fig. 17. Again, the overall prediction of the mean-velocity profiles is satisfactory while similar discrepancies can be observed as for $Re_H = 10{,}595$. When the resolution increases, the recirculation region becomes larger and stronger, so that above the recirculation, the mean streamwise velocity is overpredicted. In the recovery region, the mean velocities throughout the entire channel are improved. The turbulent kinetic energy and Reynolds shear stress are reproduced reasonably well, but show a more pronounced overprediction than for $Re_H = 10{,}595$ for both resolutions. This larger overprediction is found for the fine case $WMLES\_F37$ than for the coarse case $WMLES\_C37$, which shows that the Reynolds stresses are rather sensitive to the grid resolution.

7 Conclusions

A wall model based on the simplified TBLE has been constructed in the framework of implicit LES and an immersed-interface method for representing complex geometries on Cartesian grids. Coarsely resolved LES for turbulent channel flow at moderately large to very large Reynolds numbers show a clear improvement due to the wall model. Three different TBLE turbulence models were tested. A simple mixing length model, with an eddy viscosity depending only on the friction velocity and the wall distance, gave the best results. Alogarithmic-layer mismatch observed for large Reynolds numbers was removed by introducing a physically motivated damping function. When the grid resolution increases, the results can also be improved in the framework of LES. It was confirmed that the wall model also works properly with the immersed-interface method. For the backward-facing step flow at moderate Reynolds number, it was confirmed that for coarse LES on the one hand, the wall model improves the prediction of the mean flow, and on the other hand, it prevents the occurrence of a secondary recirculation area that can be found in the coarse LES without wall

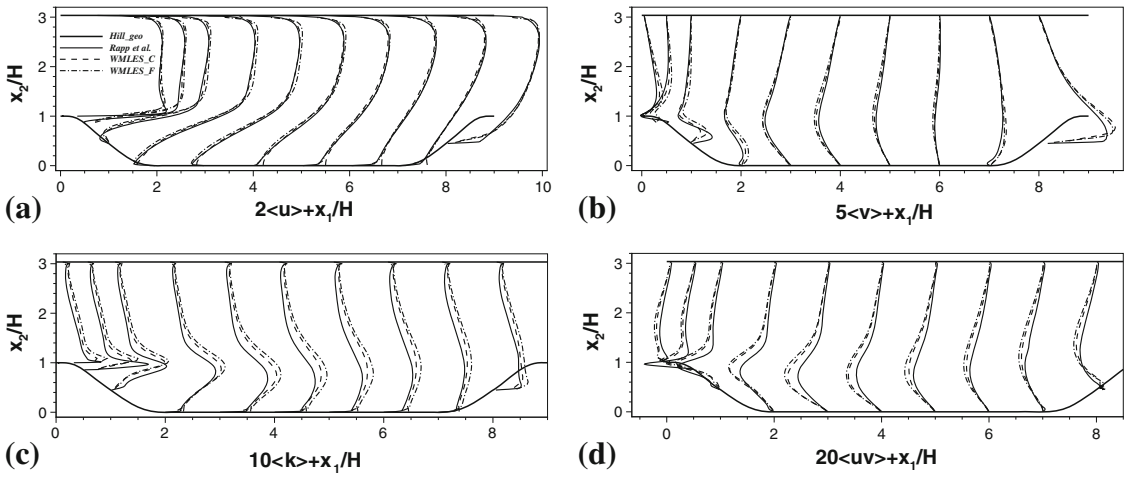

Fig. 17 Comparisons of mean-flow variables for periodic hill at $Re_H = 37{,}000$, *lines* labeled as in **a**. **a** Mean streamwise velocity, **b** mean vertical velocity, **c** turbulent kinetic energy, **d** Reynolds shear stress

model. For the massively separated flow over periodic hills at two high Reynolds numbers, the TBLE-based wall model can predict the mean flow much better than coarse LES without wall modeling and reproduce the Reynolds stresses reasonably well on very coarse grids. From the two different Reynolds numbers considered for the periodic hill, it can be seen that the prediction quality of the Reynolds stresses is more sensitive to the LES-domain resolution than that of the mean velocity. In general, our results confirm that TBLE-based wall modeling in conjunction with implicit LES and immersed-interface methods is a suitable and robust way to deal with complex geometries and flows at high Reynolds numbers, while inheriting the advantages and disadvantages of this particular kind of wall model.

Acknowledgments The authors are indebted to Dr. X. Y. Hu, Mr. M. Meyer, and Dr. C. Stemmer for valuable discussions and support. The first author gratefully acknowledges the China Scholarship Council (CSC) for financial support. This work has been supported by the WALLTURB (A European synergy for the assessment of wall turbulence) project. Partial funding was made available by the EC under the 6th framework program (CONTRACT No.: AST4-CT-2005-516008).

Appendix: The coherent structures-based model

An adaptive coefficient formulation based on the coherent structures notion [33] can be constructed by

$$\boldsymbol{\sigma}_{i,j,k} = \sigma |F_{\mathrm{CS}}|^{3/2} F_{\Omega} \boldsymbol{I}_{i,j,k}, \tag{23}$$

where $\boldsymbol{I}_{i,j,k}$ is units vector of Cartesian coordinates, and

$$\begin{aligned} F_{\mathrm{CS}} &= \frac{Q}{E}, \quad F_{\Omega} = 1 - F_{\mathrm{CS}}, \\ Q &= \frac{1}{2}\left(\overline{W}_{ij}\overline{W}_{ij} - \overline{S}_{ij}\overline{S}_{ij}\right), \\ E &= \frac{1}{2}\left(\overline{W}_{ij}\overline{W}_{ij} + \overline{S}_{ij}\overline{S}_{ij}\right), \\ \overline{W}_{ij} &= \frac{1}{2}\left(\frac{\partial \overline{u}_j}{\partial x_i} - \frac{\partial \overline{u}_i}{\partial x_j}\right), \\ \overline{S}_{ij} &= \frac{1}{2}\left(\frac{\partial \overline{u}_j}{\partial x_i} + \frac{\partial \overline{u}_i}{\partial x_j}\right), \end{aligned} \tag{24}$$

where $\overline{S}_{ij}$ and $\overline{W}_{ij}$ are the velocity-strain tensor and the vorticity tensor of the resolved flow field, respectively. F_{CS} is the coherent structure function defined as the second invariant normalized by the magnitude of the resolved velocity gradient tensor E. For incompressible flow, the second invariant $Q \propto x_2^2$ and $E \propto const$, the 3/2 power of F_{CS} scales the implicit SGS viscosity proportionally to x_2^3 near the wall.

References

1. Adams, E.W., Johnstont, J.P.: Flow structure in the near-wall zone of a turbulent separated flow. AIAA J. **26**(8), 932–939 (1988)
2. del Alamo, J.C., Jiménez, J., Zandonade, P., Moser, R.D.: Scaling of the energy spectra of turbulent channels. J. Fluid Mech. **500**, 135–144 (2004)
3. Baggett, J.S.: Some modeling requirements for wall models in large eddy simulation. CTR Annu. Res. Briefs 123–134 (1997)
4. Baggett, J.S., Jiménez, J., Kravchenko, A.: Resolution requirements in large-eddy simulation of shear flows. CTR Annu. Res. Briefs 51–66 (1997)
5. Balaras, E., Benocci, C.: Subgrid-scale models in finite-difference simulations of complex wall bounded flows AGARD 2.1–2.5 (1994)
6. Balaras, E., Benocci, C., Piomelli, U.: Two-layer approximate boundary conditions for large-eddy simulations. AIAA J. **34**, 1111–1119 (1996)
7. Baldwin, B.S., Lomax, H.: Thin Layer Approximation and Algebraic Model for Separated Turbulent Flows. AIAA paper (78-257) (1978)
8. Bhattacharya, A., Das, A., Moser, R.D.: A filtered-wall formulation for large-eddy simulation of wall-bounded turbulence. Phys. Fluids **20**, 115104-1–115104-16 (2008)
9. Brasseur, J., Wei, T.: Designing large-eddy simulation of the turbulent boundary layer to capture law-of-the-wall scaling. Phys. Fluids **22**, 021303-1–021303-21 (2010)
10. Breuer, M., Jaffrézic, B., Arora, K.: Hybrid LES-RANS technique based on a one-equation near-wall model. J. Theor. Comput. Fluid Dyn. **22**, 157–187 (2008)
11. Breuer, M., Kniazev, B., Abel, M.: Development of wall models for LES of separated flows using statistical evaluations. Comput. Fluids **36**, 817–837 (2007)
12. Cabot, W.H.: Wall models in large eddy simulation of separated flow. CTR Annu. Res. Briefs 97–106 (1997)
13. Cabot, W.H., Moin, P.: Approximate wall boundary conditions in the large-eddy simulation of high Reynolds number flows. Flow Turbul. Combust. **63**, 269–291 (1999)
14. Choi, J.I., Oberoi, R.C., Edwards, J.R., Rosati, J.A.: An immersed boundary method for complex incompressible flows. J. Comput. Phys. **224**, 757–784 (2007)
15. Cristallo, A., Verzicco, R.: Combined immersed boundary/large-eddy-simulations of incompressible three dimensional complex flows. Flow Turbul. Combust. **77**, 3–26 (2006)
16. Deardorff, J.W.: A numerical study of three-dimensional turbulent channel flow at large Reynolds numbers. J. Fluid Mech. **41**, 453–465 (1970)
17. Fadlun, E.A., Verzicco, R., Orlandi, P., Mohd-Yusof, J.: Combined immersed-boundary finite-difference methods for three-dimensional complex flow simulations. J. Comput. Phys. **161**, 35–60 (2000)
18. Fröhlich, J., Mellen, C.P., Rodi, W., Temmerman, L., Leschziner, M.A.: Highly resolved large-eddy simulation of separated flow in a channel with streamwise periodic constrictions. J. Fluid Mech. **526**, 19–66 (2005)
19. Fröhlich, J., von Terzi, D.: Hybrid LES/RANS methods for the simulation of turbulent flows. Prog. Aerosp. Sci. **44**, 349–377 (2008)
20. Fureby, C., Grinstein, F.F.: Large eddy simulation of high-Reynolds number free and wall-bounded flows. J. Comput. Phys. **181**, 68–97 (2002)
21. Garnier, E., Mossi, M., Sagaut, P., Deville, M.: On the use of shock-capturing schemes for large-eddy simulation. J. Comput. Phys. **153**, 273–311 (1999)
22. Grinstein, F.F., Fureby, C.: From canonical to complex flows: Recent progress on monotonically integrated LES. Comp. Sci. Eng. **6**, 36–49 (2004)
23. Grinstein, F.F., Margolin, L.G., Rider, W.J.: Implicit Large Eddy Simulation. Cambridge University Press, Cambridge (2007)
24. Hickel, S., Adams, N.A.: On implicit subgrid-scale modeling in wall-bounded flows. Phys. Fluids **19**, 105106-1–105106-13 (2007). doi:10.1063/1.2773765
25. Hickel, S., Adams, N.A.: A proposed simplification of the adaptive local deconvolution method. Eur. Ser. Appl. Ind. Math. **16**, 66–76 (2007). doi:10.1051/proc:2007008
26. Hickel, S., Adams, N.A.: Implicit LES applied to zero-pressure-gradient and adverse-pressure-gradient boundary-layer turbulence. Int. J. Heat Fluid Flow **29**(3), 626–639 (2008). doi:10.1016/j.ijheatfluidflow.2008.03.008
27. Hickel, S., Adams, N.A., Domaradzki, J.A.: An adaptive local deconvolution method for implicit LES. J. Comput. Phys. **213**, 413–436 (2006). doi:10.1016/j.jcp.2005.08.017
28. Hoyas, S., Jiménez, J.: Scaling of the velocity fluctuations in turbulent channels up to $Re_\tau = 2003$. Phys. Fluids **18**, 011702-1–011702-4 (2006)
29. Hutchins, N., Marusic, I. (2007) Large-scale influences in near-wall turbulence. Philos. Trans. R. Soc. A **365**, 647–664
30. Jovic, S.: An Experimental Study of a Separated/Reattached Flow Behind a Backward-Facing Step. $Re_h = 37{,}000$. NASA TM 110384 (1996)
31. Jovic, S., Driver, D.M.: Backward-Facing Step Measurements at Low Reynolds Number, $Re_h = 5000$. NASA TM 108807 (1994)
32. Kang, S., Iaccarino, G., Ham, F., Moin, P.: Prediction of wall-pressure fluctuation in turbulent flows with an immersed boundary method. J. Comput. Phys. **228**, 6753–6772 (2009)
33. Kobayashi, H., Ham, F., Wu, X.: Application of a local SGS model based on coherent structures to complex geometries. Int. J. Heat Fluid Flow **29**(3), 640–653 (2008)
34. Le, H., Moin, P., Kim, J.: Direct numerical simulation of turbulent flow over a backward-facing step. J. Fluid Mech. **330**, 349–74 (1997)
35. Meyer, M., Devesa, A., Hickel, S., Hu, X.Y., Adams, N.A.: A conservative immersed interface method for large-eddy simulation of incompressible flows. J. Comput. Phys. **18**, 6300–6317 (2010). doi:10.1016/j.jcp.2010.04.040

36. Meyer, M., Hickel, S., Adams, N.A.: Assessment of implicit large-eddy simulation with a conservative immersed-interface method for turbulent cylinder flow. Int. J. Heat Fluid Flow. **31**, 368–377 (2010). doi:10.1007/978-3-642-13872-0_12
37. Mittal, R., Iaccarino, G.: Immersed boundary methods. Annu. Rev. Fluid Mech. **37**, 239–261 (2005)
38. Moser, R.D., Kim, J., Mansour, N.N.: Direct numerical simulation of turbulent channel flow up to $Re_\tau = 590$. Phys. Fluids **11**(4), 943–945 (1999)
39. Nicoud, F., Baggett, J.S., Moin, P., Cabot, W.: Large eddy simulation wall-modeling based on suboptimal control theory and linear stochastic estimation. Phys. Fluids **13**(10), 2968–2984 (2001)
40. Piomelli, U.: Wall-layer models for large eddy simulations. Prog. Aerosp. Sci. **44**, 437–446 (2008)
41. Piomelli, U., Balaras, E.: Wall-layer models for large-eddy simulation. Annu. Rev. Fluid Mech. **34**, 349–374 (2002)
42. Piomelli, U., Moin, P., Ferziger, J.H., Kim, J.: New approximate boundary conditions for large-eddy simulations of wall-bounded flows. Phys. Fluids A **1**, 1061–1068 (1989)
43. Rapp, C., Breuer, M., Manhart, M., Peller, N.: 2D Periodic Hill Flow. http://qnet.cfms.org.uk (2010)
44. Roman, F., Armenio, V., Fröhlich, J.: A simple wall-layer model for large eddy simulation with immersed boundary method. Phys. Fluids **12**, 101701-1–101701-4 (2009)
45. Schumann, U.: Subgrid scale model for finite difference simulations of turbulent flows in plane channels and annuli. J. Comput. Phys. **18**, 376–404 (1975)
46. Stolz, S., Adams, N.A.: An approximate deconvolution procedure for large-eddy simulation. Phys. Fluids **11**(4), 1699–1701 (1999)
47. Temmerman, L., Leschziner, M.A., Mellen, C.P., Fröhlich, J.: Investigation of wall-function approximations and subgrid-scale models in large-eddy simulation of separated flow in a channel with periodic constrictions. Int. J. Heat Fluid Flow **24**, 157–180 (2003)
48. Tessicini, F., Iaccarino, G., Wang, M., Verzicco, R.: Wall modeling for large-eddy simulation using an immersed-boundary method. CTR Annu. Res. Briefs 181–187 (2002)
49. Šarić, S., Jakirlić, S., Breuer, M., Jaffrézic, B., Deng, G., Chikhaoni, O.: Evaluation of detached-eddy simulations for predicting the flow over periodic hills. In: Cancès, E., Gerbeau, J.F. (eds.) ESAIM Proceedings CEMRACS 2005: Computational aeroacoustics and computational fluid dynamics in turbulent flows. Marseille, France (July 18–August 26, 2005)
50. Wang, M., Moin, P.: Dynamic wall modeling for large-eddy simulation of complex turbulent flows. Phys. Fluids **14**(7), 2044–2051 (2002)